EuroSun2026

LIFE CYCLE ASSESSMENT OF TWO FLOATING PHOTOVOLTAIC SYSTEMS WITH FOCUS ON FLOATING SUBSTRUCTURES

Felix Brach (corresponding author), Joachim Göttsche, Nico Oellers, Daniel Schmitz, Niyousha Karami

Solar-Institut Jülich, FH Aachen University of Applied Sciences, Jülich (Germany)

brach@sij.fh-aachen.de

Summary

Floating photovoltaic (FPV) systems offer a promising opportunity to expand solar energy production without competing for land resources. This study assesses the life cycle greenhouse gas emissions of two commercial FPV systems in North Rhine-Westphalia, Germany, complemented by a small-scale prototype, in accordance with ISO 14040 and ISO 14044. Over a 20-year service life, the carbon footprints amount to 120.2 and 87.7 g CO_2-eq / kWh. PV modules dominate both balances, and the floating substructure and the modules contribute in roughly equal parts to the difference between the two systems. Since the module contribution follows the supply chain and the module generation installed rather than the structural concept, an additional indicator is introduced that relates the emissions of the floating substructure to its load-bearing capacity. On this basis the steel design requires 862.1 g CO_2-eq / kg, the steel–HDPE design 398.6 g CO_2-eq / kg and the prototype 729.1 g CO_2-eq / kg. The hybrid design is thus 53.8% below the steel design, roughly twice the margin found at system level. The indicator is independent of site and of an assumption regarding energy yield, and it therefore allows structural concepts to be compared directly.

Floating photovoltaics, FPV, LCA, life cycle assessment, carbon footprint, floating substructure, solar energy

Field of application for the findings: Sustainable and Solar Energy Transition

Addressed audience: Researchers, FPV system developers, environmental analysts, renewable energy planners

1. Introduction

The expansion of photovoltaic generation increasingly competes for land. Agricultural areas, nature conservation and settlement development limit the sites available for ground-mounted systems, particularly in densely populated regions. Floating photovoltaic systems address this constraint by using water surfaces that serve no competing purpose, such as reservoirs, irrigation basins and flooded gravel pits. Beyond avoiding land use, they offer further advantages, including reduced evaporation from the water body and lower operating temperatures, which can improve module efficiency (Cagle et al., 2020; Cazzaniga et al., 2018).

The segment has grown accordingly. Worldwide installed capacity has risen from a negligible level in 2015 to more than 9.6 GWp by 2024, while the estimated technical potential exceeds 22 TWp on a tenth of the world's inland water bodies alone (Gandhi et al., 2026). Germany shows both the enthusiasm and the challenges involved. Since January 2023 the Federal Water Act has permitted floating installations only on artificial or substantially modified water bodies, has limited them to 15% of the water surface and has required a minimum distance of 40 m from the shore (Federal Republic of Germany, 2023). These provisions restrict the choice of site and the size of an installation. The systems examined in this study are located on flooded gravel pits.

Compared with ground-mounted systems, the distinguishing component of a floating installation is the substructure. It has to provide buoyancy, transfer the loads of modules, cabling and inverters, withstand wind and wave action and resist corrosion in a permanently humid environment. These requirements are met by markedly different design concepts. Some manufacturers use HDPE floats carried by a metal frame, whereas others use steel bodies that provide buoyancy and load transfer at the same time. The choice affects material demand, installation effort and durability, and it is the aspect of a floating system over which a designer has the greatest influence.

Life cycle assessments of floating installations remain comparatively rare, and those available focus on complete systems. Published results range from 28 to 102 g CO_2-eq / kWh (Cromratie Clemons et al., 2021; Kester et al., 2024; Frehner et al., 2024), a spread of roughly a factor of four that reflects differences in modules, site conditions and modelling assumptions rather than differences between structural concepts. This is a consequence of the functional unit: relating emissions to a kilowatt-hour makes the result depend on module efficiency, orientation, irradiation and plant size. In the two commercial systems examined here, PV modules account for 68.5 and 78.3% of the total, and shares of 60 and 61% are reported for the two operational systems assessed by Kester et al. (2024). A comparison on this basis therefore largely measures the choice of module. That choice, however, follows the global supply chain and the module generation available at the time of construction, and it is essentially independent of how the system floats.

An assessment that seeks to compare structural concepts therefore requires a different reference quantity. This study assesses two commercial floating photovoltaic systems in North Rhine-Westphalia, Germany, and a small-scale prototype. Both commercial systems are first assessed completely, which establishes the context and quantifies the contribution of each component group. The scope is then narrowed to the floating substructures, and an additional indicator is introduced that relates their emissions to the load-bearing capacity they provide. This quantity follows from the displacement of the buoyancy bodies and the dead weight of the substructure alone. It is independent of site and of an assumption regarding energy yield, and it therefore isolates the structural concept from the factors that dominate system-level results.

No published assessment was found that applies such a functional unit to floating substructures. This work therefore contributes in two ways. It provides life cycle data for two operational systems whose substructures differ fundamentally, and it proposes an indicator that makes their structural efficiency directly comparable. Section 2 describes the systems and the methodology, Section 3 reports the results at system and substructure level, and Section 4 discusses the design implications and places the results in the context of published assessments.

2. Methodology

2.1 Description of the assessed systems

Three floating photovoltaic installations in North Rhine-Westphalia, Germany, form the basis of this study. Two of them are commercial systems operated on flooded gravel pits and are assessed in full. The third is a small-scale prototype. It is included only in the comparison of floating substructures in Section 3.3, and no system-level results are reported for it. Tab. 1 summarises their characteristics.

Tab. 1: Key characteristics of the assessed floating photovoltaic systems. Azimuth angles follow the PVGIS convention, in which 0° denotes south, negative values east and positive values west.

Parameter	FPV1	FPV2	Prototype
Installed capacity (kWp)	739.4	494.1	17.4
Number of modules	1872	810	30
Module rating (Wp)	395	610	580
Tilt angle (°)	12	10	15
Azimuth (°)	−82 / +98	+50 / −130	−90 / +90
Buoyancy bodies	Galvanised steel	HDPE	HDPE and stainless steel
Substructure materials	Galvanised steel, aluminium	Galvanised steel, HDPE	Aluminium, stainless steel, HDPE
Module mounting	Aluminium	Steel	Aluminium
Load-bearing capacity (t)	396.4	216.8	8.68

The three systems differ mainly in how buoyancy is provided and how the modules are attached. In FPV1 the buoyancy bodies are galvanised steel floats with an epoxy resin coating. They are connected to one another either directly or through additional galvanised steel members. The mounting profiles that carry the modules are made of aluminium and are bolted onto these connecting structures. FPV2 uses a hybrid design. Buoyancy is provided by discrete HDPE floats held in a galvanised steel frame that also carries the walkways, the module mounting and the inverter platforms. FPV2 is the only one of the three systems in which the module mounting is an integral part of the frame rather than a separate component. The prototype follows a third approach. Buoyancy is provided by HDPE pipes attached beneath an aluminium truss. A folding mechanism is mounted on top of this truss and carries the mounting profiles and the modules. The mechanism is unfolded on site and locked in position once the system is deployed.

In all three installations the modules are mounted in two opposing orientations at a shallow tilt, an arrangement chosen to reduce wind loads and mutual shading and to flatten the daily generation profile. The substructures are held in position by anchoring systems consisting of steel cables, clamps, shackles and anchors.

2.2 Goal, scope and system boundaries

The study pursues two goals. The first is to quantify the life cycle greenhouse gas emissions of the two commercial systems and to identify the component groups that govern them. The second is to compare the floating substructures of all three installations on a basis that is independent of electricity generation, so that structural design concepts can be evaluated against one another. No critical review in the sense of ISO 14044 was carried out. The results describe three individual installations, which are not identified by manufacturer or product, and are not intended as a claim about the environmental superiority of commercially available floating substructures.

The assessment follows ISO 14040 and ISO 14044 and covers raw material extraction, component manufacturing, transport to the site and installation (International Organization for Standardization, 2006a,b). The inventory comprises PV modules, inverters, electrical components, the floating substructure, anchoring elements and transport.

Two life cycle stages are deliberately excluded. Maintenance during operation was not included, because its extent varies widely between projects and no reliable data were available. End-of-life treatment was likewise not modelled. All three installations are still in operation, so no dismantling data exist, and the recycling routes available in 20 to 30 years cannot be anticipated with the processes documented today. The results reported here are therefore cradle-to-gate figures, extended by transport to the site and installation, rather than cradle-to-grave figures. Under the cut-off system model applied here, no credits for recycling accrue to the producer of the waste, so including an end-of-life stage could only increase the results. Under a system model that accounts for avoided primary production, the sign of that contribution can differ. The comparison studies discussed in Section 4.2 do model end-of-life treatment and report it as a relevant contributor. Both limitations are addressed in Section 4.3.

A service life of 20 years was used as the base case, with 25 and 30 years assessed additionally. For the two longer service lives a single replacement of the inverters after 15 years was assumed. Field data on 2121 inverters in residential and small commercial systems show that 34.3% of them suffered a first energy-relevant failure within 15 years, so that roughly two thirds are still operating without fault at that point (Bucher et al., 2022). Replacing every inverter after 15 years is therefore a conservative assumption. Because only a single replacement is assumed, the absolute emissions are identical for the 25- and 30-year cases, and only the cumulative electricity generation increases.

Two boundary decisions deserve explicit mention because they affect the comparison of substructures.

Extent of the floating substructure. The substructure was defined as everything between the water surface and the underside of the modules. This includes the buoyancy bodies and the supporting structure, but neither the modules themselves nor the electrical equipment, which are treated as payload. The mounting is implemented differently in each system. In FPV1 the mounting profiles are made of aluminium and are bolted onto steel connecting members that join the buoyancy bodies. They can be removed without affecting the load-bearing capacity of the substructure. In FPV2 the profiles are made of steel and are bolted directly to the steel frame that also holds the floats, so that the mounting and the frame form a single steel assembly. In the prototype the aluminium profiles sit on the folding mechanism and contribute to its stability. Removing them would leave the folding mechanism unstable and with it the part of the structure that carries the modules, although the aluminium frame attached to the buoyancy pipes would remain unaffected.

The mounting was nonetheless assigned to the substructure in all three cases, so that the boundary sits at the same physical location in every system. Assigning it to the payload instead would make the comparison depend on how far a particular design integrates the mounting into the frame, and on how finely a manufacturer happens to itemise the parts list.

Machinery used during installation. For FPV1 the use of a telehandler during assembly on site was included. It accounts for 1.1% of the total emissions of that system. For FPV2 and the prototype no such process was included, because assembly was carried out by hand on site. This is not a difference in data coverage but a consequence of the design. The heavy steel buoyancy bodies of FPV1 cannot be launched by hand, whereas HDPE floats can. The point is taken up again in Section 4.1.

2.3 Functional units

System-level results are reported as greenhouse gas emissions in CO_2-eq per kilowatt-hour of electricity generated over the assumed service life. This is the established reference unit for electricity generation technologies and allows comparison with other photovoltaic systems. Results per kilowatt-peak of installed capacity are reported as well, because this unit is independent of site-specific irradiation.

Neither unit, however, allows a meaningful comparison of floating substructures. Both relate emissions to the electrical output of the system and are therefore governed by module efficiency and module rating, the kilowatt-hour additionally by orientation and local irradiation. None of these quantities affects how efficiently a structure provides buoyancy.

The modules deserve particular attention here, because they dominate the system-level results and at the same time lie largely outside the designer's control. About 96% of the solar modules and their components produced in 2025 originated in Asia (Fraunhofer Institute for Solar Energy Systems ISE, 2026), so their footprint is set by the supply chain rather than by the installation concept. Module technology also advances rapidly, so two installations built in different years differ in their specific emissions for reasons that have nothing to do with how they float.

An additional indicator is therefore introduced that relates the emissions of the floating substructure to its load-bearing capacity:

$$I_{\mathrm{sub}} = \frac{m_{\mathrm{GHG,sub}}}{m_{\mathrm{cap}}} \tag{1}$$

where I_{sub} is the specific impact in $\mathrm{g\,CO_2\text{-}eq/kg}$, $m_{\mathrm{GHG,sub}}$ the life cycle greenhouse gas emissions of the substructure, that is its material and manufacturing emissions without delivery and installation, and m_{cap} its load-bearing capacity. The latter was determined using Archimedes' principle as the mass of water displaced by the buoyancy bodies, reduced by the dead weight of the floating substructure itself:

$$m_{\mathrm{cap}} = \rho_{\mathrm{w}}\, V_{\mathrm{sub}} - m_{\mathrm{struct}} \tag{2}$$

with ρ_{w} the density of fresh water, V_{sub} the volume of the buoyancy bodies and m_{struct} the mass of all permanently installed structural components. Strictly speaking this quantity is the net buoyancy at full submersion rather than a structurally verified carrying capacity. It is used here as a simplified proxy, because it follows from geometry and mass in the same way for all three installations. A structural verification would require load cases and safety factors that are not documented for any of them. Full submersion of the buoyancy bodies is assumed, so that the indicator refers to the theoretical maximum load-bearing capacity. The same convention is applied to all three installations. PV modules, electrical equipment and anchoring were treated as payload and were not deducted. The indicator thus expresses the greenhouse gas emissions caused per kilogram of load-bearing capacity provided on the water surface.

Two properties make this indicator useful beyond the present study. It is independent of the site, so that installations on different water bodies can be compared directly. It also depends on no assumption regarding energy yield, and is therefore unaffected by simulation settings, degradation rates, system losses and the assumed service life.

2.4 Life cycle inventory and data sources

The foreground inventory was based on primary data. For each installation, the parts lists were provided by the operator of the plant. For FPV1 the operator also designed and built the floating substructure, whereas the substructure of FPV2 was purchased from a manufacturer. Where a component was documented without its mass, the mass was derived from the dimensions given in the parts lists and the density of the material. This applied mainly to structural elements of the floating substructures. For standardised parts such as screws, clamps and shackles, published manufacturer data were used instead. The components were then assigned to the component groups reported in Section 3.

Background data were taken from ecoinvent 3.12 using the allocation, cut-off by classification system model (Ecoinvent Association, 2025), and the models were built in SimaPro 10.2.0.2. Under this system model recyclable materials enter a product system free of the burdens of their primary production, and the burden of a waste treatment is assigned to the producer of the waste. Two processes required additional modelling because no suitable dataset was available.

Large parts of both floating substructures are made of galvanised steel, for which the database contains no single dataset. This concerns the buoyancy bodies and the connecting members of FPV1 and, in FPV2, the entire steel frame including the walkways and the module mounting. The steel was therefore modelled using the dataset for unalloyed steel, and the zinc coating was added as a separate material input. The epoxy coating of the FPV1 buoyancy bodies is included in that assembly. The zinc mass was obtained from the coated surface area, the thickness of the coating and the density of zinc.

The background datasets already include the average transport of the materials to the point of use. The transport reported separately as a component group covers the delivery of the components to the site. For FPV1 it was modelled from primary data, because the buoyancy bodies were manufactured by the operator and taken from the operator's workshop to the water body.

The database likewise contained no dataset for the inverters actually installed. They were therefore modelled by combining as many units of a smaller inverter dataset as were needed to match the rated power of the installed device.

The load-bearing capacity in Equation (2) was determined in the same way for all three installations, from the geometry of the buoyancy bodies and the dead weight of the floating substructure. Tab. 2 summarises the resulting quantities. The dead weight comprises every permanently installed structural component of the floating platform, whereas modules, electrical equipment and anchoring are treated as payload in all three cases. The last row relates the two, and thus states how much payload each design carries per unit of its own structural mass.

Tab. 2: Derivation of the load-bearing capacity from displaced volume and dead weight. The buoyancy bodies of FPV1 measure 12 m × 0.667 m × 0.667 m, those of the prototype consist of a 5.5 m central pipe and three coiled pipes of 11 m each at a radius of 0.1 m. For the prototype the displaced volume is an approximation: the pipes are corrugated, and the calculation uses the envelope of a smooth cylinder of 200 mm diameter, so the value is an upper bound.

Quantity	FPV1	FPV2	Prototype
Buoyancy bodies	99 steel floats	296 HDPE floats	8 pipe coils
Volume per body (m^3)	5.339	0.847	1.210
Displaced volume (m^3)	528.6	250.7	9.68
Displaced mass (t)	528.6	250.7	9.68
Dead weight (t)	132.1	33.9	1.00
Load-bearing capacity (t)	396.4	216.8	8.68
Payload per dead weight (kg/kg)	3.0	6.4	8.7

2.5 Impact assessment and yield simulation

Environmental impacts were calculated with the Environmental Footprint 3.1 (adapted) V1.03 method at the characterisation level (European Commission, 2022). The method was developed by the European Commission within the Product Environmental Footprint initiative and is widely used in European assessments. Results are therefore comparable with other studies that apply the same framework. Only the impact category climate change is reported, expressed as GWP100. The assessment is therefore single-issue: possible trade-offs in other categories, in particular those driven by the aluminium and stainless steel content of the substructures, were not examined.

The electricity generation needed to relate the results to a kilowatt-hour was simulated with PVGIS (European Commission, 2025). Each installation was modelled as two equal halves corresponding to its two module orientations, using the tilt and azimuth angles given in Tab. 1 and a flat system loss of 10%. This value covers cabling and inverter losses, soiling and reduced module performance at elevated temperatures. It was set below the PVGIS default of 14%, because the default already contains an allowance for average module degradation (European Commission, 2025). In this study the degradation is applied explicitly, as described below. Lowering the flat loss therefore prevents degradation from being counted twice.

Module degradation was derived from the linear performance warranty of the module type actually installed. The same rule was applied to all three systems:

$$d = \frac{100\,\% - P_{\mathrm{res}}}{n_{\mathrm{war}}} \tag{3}$$

where P_{res} is the residual power guaranteed at the end of the warranty period and n_{war} the length of that period. The resulting rates are given in Tab. 3. They differ between the systems because the warranties differ, not because different methods were applied. Because a warranty states the minimum power retained, it yields an upper bound on the degradation rate. Measured degradation rates of crystalline silicon modules are typically lower, with a reported median of about 0.5% per year (Jordan and Kurtz, 2013). Since the same rule was applied to all three systems, this does not distort the comparison.

Tab. 3: Yield simulation input and resulting cumulative electricity generation. The degradation rate follows from Equation (3) and the warranty of the installed module type.

Input quantity	FPV1	FPV2	Prototype
Warranted residual power	80.7%	87.4%	88.0%
Warranty period (years)	25	30	30
Degradation rate (%/a)	0.772	0.420	0.400
System losses (%)	10	10	10
E_0 (MWh)	671.46	449.43	15.99
E_{20} (MWh)	12 489	8639	308
E_{25} (MWh)	15 320	10 687	381
E_{30} (MWh)	18 043	12 693	453

The cumulative electricity generation over a service life of n years is given by Equation (4):

$$E_n = \sum_{k=0}^{n-1} E_0\,(1-d)^k \tag{4}$$

with E_0 the yield of the first year without degradation.

3. Results

3.1 Life cycle emissions of the complete systems

Over the 20-year base case, FPV1 causes 120.2 g CO_2-eq / kWh and FPV2 87.7 g CO_2-eq / kWh. The emissions of the hybrid system are therefore 27.0% lower per unit of electricity generated. Per installed capacity the values are 2029 and 1534 kg CO_2-eq per kWp.

Fig. 1 shows how these totals per kilowatt-hour are composed. PV modules dominate in both systems, contributing 68.5% in FPV1 and 78.3% in FPV2. The floating substructure follows with 22.8% and 11.4% respectively. No other component group exceeds 5%. Electrical components and inverters contribute almost identical absolute amounts in both systems, between 4.1 and 4.3 g CO_2-eq / kWh, while anchoring and transport together account for less than 0.8 g CO_2-eq / kWh in either case.

Decomposing the difference of 32.4 g CO_2-eq / kWh between the two systems is more informative than the totals themselves. The floating substructure accounts for 17.4 g CO_2-eq / kWh or 53.5% of the difference, the PV modules for 13.7 g CO_2-eq / kWh or 42.2%, and the telehandler used during installation of FPV1 for the remaining 1.3 g CO_2-eq / kWh or 4.1%. Electrical components, inverters, anchoring and transport cancel each other almost completely and jointly contribute less than 0.1 g CO_2-eq / kWh.

The module contribution is not attributable to the structural design. It follows from the different module generations installed, from the higher rated power per unit at FPV2 and from the different specific yields of the two sites. The substructure and the installation process, by contrast, follow directly from how the system was designed and built, and together they account for 57.7% of the difference. This is the practical reason for narrowing the scope in Section 3.3.

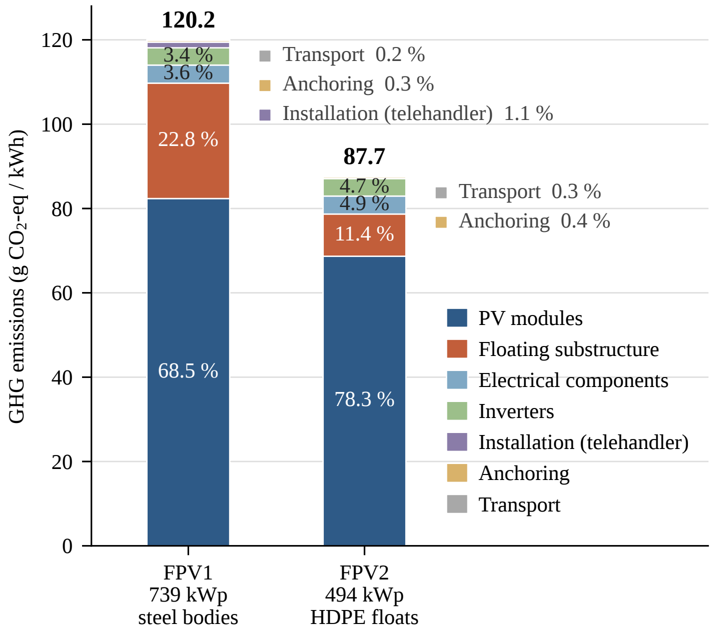

Fig. 1: Life cycle greenhouse gas emissions of the two floating photovoltaic systems per kilowatt-hour generated, by component group, assuming a 20-year service life. Percentages denote each group's share of the system total.

3.2 Sensitivity to the assumed service life

Fig. 2 shows the results for 20, 25 and 30 years of operation. Emissions per kilowatt-hour fall from 120.2 to 101.4 and 86.1 g CO_2-eq / kWh for FPV1, and from 87.7 to 74.3 and 62.5 g CO_2-eq / kWh for FPV2. Extending the assumed service life from 20 to 30 years therefore lowers the specific emissions by roughly 28% in both cases.

The reduction is not proportional to the added years. Between 20 and 25 years the inverter replacement adds emissions that partly offset the additional electricity generated, whereas between 25 and 30 years no further replacement was assumed and the full benefit of the longer operation applies.

What matters for the comparison is that the relative difference between the two systems is almost independent of this assumption. It amounts to 27.0%, 26.7% and 27.3% for 20, 25 and 30 years. The absolute values therefore depend strongly on the assumed service life, whereas the difference between the two systems does not.

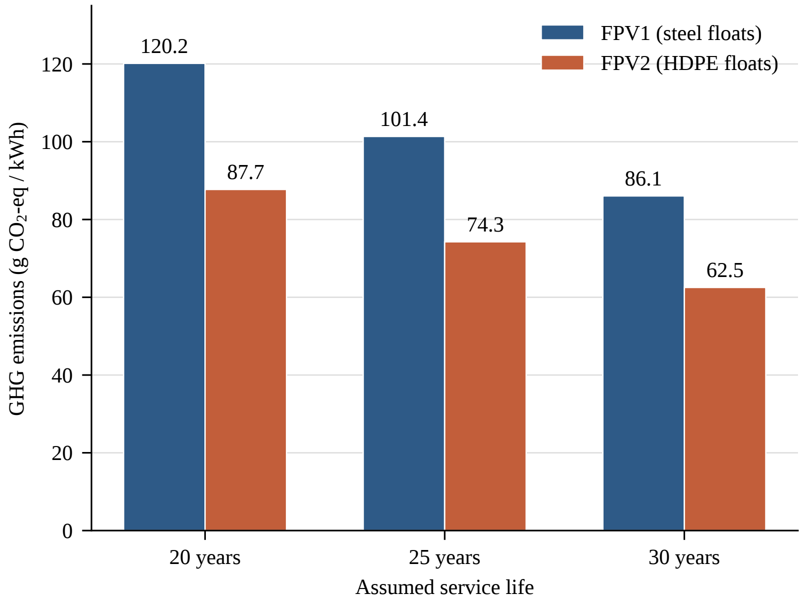

Fig. 2: Life cycle greenhouse gas emissions per kilowatt-hour generated, for an assumed service life of 20, 25 and 30 years.

3.3 Substructure emissions per unit of load-bearing capacity

Fig. 3 shows the substructures evaluated with the indicator defined in Equation (1). FPV1 causes 862.1 g CO_2-eq / kg of load-bearing capacity, FPV2 398.6 g CO_2-eq / kg and the prototype 729.1 g CO_2-eq / kg. The hybrid design of FPV2 is thus 53.8% below the steel design of FPV1, a margin considerably larger than the 27.0% found at system level. Removing the modules and the electrical equipment from the comparison makes the structural difference fully apparent.

The decisive finding lies in how the total splits between the two structural functions. The steel buoyancy bodies of FPV1 account for 627.9 g CO_2-eq / kg, whereas the HDPE ones of FPV2 account for only 119.3 g CO_2-eq / kg. Providing buoyancy with HDPE is therefore less emission-intensive by a factor of 5.3 per unit of load-bearing capacity than providing it with steel. The ranking is reversed for the supporting structure, which accounts for 234.3 g CO_2-eq / kg in FPV1 but 279.2 g CO_2-eq / kg in FPV2. The two systems distribute the structural work differently. FPV1 has no frame in the conventional sense. Its steel bodies provide buoyancy and carry the loads at the same time, so that only connecting elements between the bodies and the mounting profiles are needed in addition. In FPV2 the floats provide buoyancy and in places also serve as a walking surface, but the load transfer is carried by a separate steel structure, which adds mass that contributes nothing to buoyancy. Where the floats are not walkable, steel grating is fitted in addition.

The trade-off is therefore not between steel and plastic as such, but between integrating buoyancy and load transfer into one component or separating them. Separation pays off in the present case, since the penalty on the supporting structure is far smaller than the saving on the buoyancy bodies.

Steel still dominates the FPV2 substructure. Its steel components account for 68.4% of the substructure emissions, the HDPE floats for 29.9% and a set of HDPE pipes carried on a dedicated pontoon for the remaining 1.6%. The advantage of the hybrid design therefore does not arise from avoiding steel, but from needing considerably less of it.

The prototype confirms the pattern at a much smaller scale and with a third material combination. Its buoyancy bodies account for 233.1 g CO_2-eq / kg and the supporting structure for 496.0 g CO_2-eq / kg. The latter comprises the aluminium frame, the folding mechanism, the bolted connections and the grating that serves as a walkway.

Its high share reflects the folding mechanism, which adds structure without contributing to buoyancy, and the aluminium it is built from. With 8677 kg of load-bearing capacity against 216 842 kg for FPV2, the prototype also illustrates that the indicator remains meaningful across a factor of 25 against FPV2 and 46 against FPV1.

The buoyancy bodies of the prototype deserve a closer look, because they were modelled with the same HDPE dataset as those of FPV2 yet cause 233.1 g CO_2-eq / kg against 119.3 g CO_2-eq / kg. Three causes combine: per cubic metre of buoyancy the prototype needs 50.2 kg of polymer against 36.5 kg for the moulded floats of FPV2, because a long thin pipe has to enclose its volume with far more wall area than a compact body. Couplers, spacers and sealing rings, which have no equivalent in the moulded floats of FPV2, add a further 4% to the polymer mass. Above all, each of the eight buoyancy bodies consists of four pipes that have to be clamped together and given a fixing point at their centre. The eight bodies consist of a straight central pipe and three coiled pipes each. The clamps, wire ropes, bolts and connecting plates required for this amount to 14.8 kg of stainless steel per body and 118.7 kg in total, which alone accounts for 29% of the buoyancy-body emissions. Per kilogram of load-bearing capacity the prototype uses 72.1 g of buoyancy material against 42.2 g for FPV2, a factor of 1.71. The emissions differ by a factor of 1.95, the additional gap arising from the stainless steel, which is 1.75 times as emission-intensive per kilogram as HDPE. A buoyancy body formed in one piece therefore avoids not only material but also the need for jointing. The prototype nonetheless carries more payload per unit of dead weight than either commercial system, because the penalty lies in its buoyancy bodies rather than in the structure as a whole.

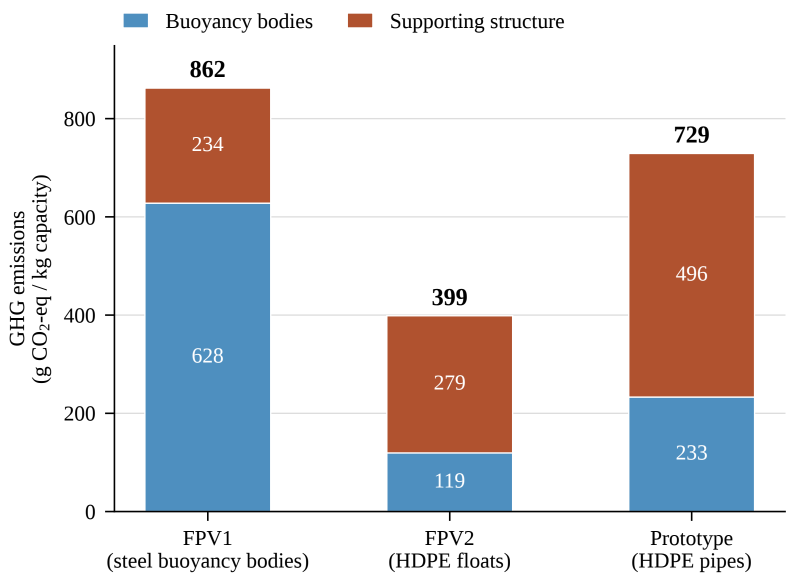

Fig. 3: Greenhouse gas emissions of the floating substructures per kilogram of load-bearing capacity, separated into the buoyancy bodies and the supporting structure. The latter comprises the frame, the walkways and the module mounting, and in addition the cable trays in FPV1 and the HDPE piping in FPV2.

4. Discussion

4.1 Material choice and installation logistics

The comparison of the three substructures suggests that the decisive design question is whether buoyancy and load transfer are handled by the same component or by separate ones. In FPV1 the steel bodies provide both at once, which keeps the supporting structure lean at 234.3 g CO_2-eq / kg but makes the buoyancy bodies emission-intensive at 627.9 g CO_2-eq / kg. FPV2 separates the two functions and pays for it with a structure that costs more per unit of capacity, at 279.2 g CO_2-eq / kg, yet its buoyancy bodies drop to 119.3 g CO_2-eq / kg. The penalty on the supporting structure amounts to 44.9 g CO_2-eq / kg, the saving on the buoyancy bodies to 508.5 g CO_2-eq / kg. Separation is therefore worthwhile by a wide margin in the cases examined here.

The prototype shows that separation alone is not sufficient. It also separates the two functions, using HDPE pipes for buoyancy, yet reaches 729.1 g CO_2-eq / kg and thus stays far above the 398.6 g CO_2-eq / kg of the hybrid design. Its supporting structure alone accounts for 496.0 g CO_2-eq / kg, more than twice that of FPV1. The folding mechanism serves deployment rather than load transfer. Its mass is small, but it is aluminium: the folding frame, the truss and the module rails together amount to 298 kg, and at 13.2 kg CO_2-eq per kilogram they account for 454 of those 496.0 g CO_2-eq / kg, more than five times what the same mass of galvanised steel would cause. The prototype therefore pays for its deployability not in mass but in material choice. A separated design is thus only advantageous if the supporting structure remains lean and is built from a material whose emission intensity matches the structural work it performs.

The structural concept has a second consequence that is not apparent from the material inventory. The steel bodies of FPV1 cannot be launched by hand and required a telehandler for assembly, which adds 1.1% to the emissions of that system. At FPV2 the floats and the steel structure were joined by hand at the water body. The prototype follows a third route. Only the aluminium truss and the buoyancy pipes are assembled on site, after which the pre-assembled folding structure is drawn out of a transport container onto them and unfolds. The container is not part of the inventory, because it is reusable and is not tied to the service life of a single installation. The additional emissions are modest in all three cases, but they show that the structural concept propagates into the installation process. For larger installations, or for sites with difficult access, this effect can be expected to grow.

Taken together, the three systems indicate where the largest reductions can be found. In all of them the buoyancy bodies and the supporting structure determine the result. Structure that serves neither buoyancy nor load transfer, such as the folding mechanism of the prototype, is the most expensive addition per unit of load-bearing capacity, particularly when it is built from an emission-intensive material. Such a design may, however, offer advantages that the indicator does not capture: rapid deployment, transportability or the option of relocating the installation. Whether these advantages outweigh the additional structural mass was not examined in this study.

4.2 Comparison with published FPV assessments

The published literature on life cycle assessments of operational FPV systems remains limited. The most directly comparable study is the IEA PVPS Task 12 report, which examines two operational installations on inland waters in Western Europe, one with HDPE floats and one with a steel–HDPE construction (Kester et al., 2024). It reports 49 and 55 g CO_2-eq / kWh over a 30-year service life, against 86.1 and 62.5 g CO_2-eq / kWh obtained here.

The difference is dominated by the PV modules rather than by the structures. That study models modules at 780 kg CO_2-eq per kWp, whereas the ecoinvent datasets used here correspond to 1391 kg CO_2-eq per kWp for FPV1 and 1201 kg CO_2-eq per kWp for FPV2. The specific yields, by contrast, are of comparable magnitude. Averaged over the same 30-year service life, that study models 889 and 795 kWh per kWp per year against 813 and 856 kWh per kWp per year here. This supports the argument developed in Section 2.3: comparisons expressed per kilowatt-hour are governed by the module inventory to an extent that makes them unsuitable for evaluating structural concepts.

The same report points in the same direction on the structural side, although the individual systems cannot be paired directly. Within each study the more steel-based of the two systems carries the higher structural share: 27% against 17% in the referenced report, and 22.8% for FPV1 against 11.4% for FPV2 here. A closer comparison of the two steel–HDPE systems would require knowing how each design distributes buoyancy and load transfer between its components, which the referenced report does not document in that detail.

Two further studies illustrate the width of the reported range. An assessment of a high-altitude installation reports 94 g CO_2-eq / kWh at a specific yield of 1388 kWh per kWp per year and identifies the modules and the mounting system as the two dominant contributors. The mounting system alone accounts for 46% of the global warming potential there, which the authors attribute to the quantity of aluminium required (Frehner et al., 2024). A study of a pontoon-based system in Thailand reports 73 g CO_2-eq / kWh (Cromratie Clemons et al., 2021).

Part of the reported spread does not come from the systems at all. Kester et al. (2024) re-evaluated two design studies against a consistent lifetime energy output per kWp and thereby moved them from 11 to 28 and from 73 to 102 g CO_2-eq / kWh respectively. The uncorrected range of 11 to 102 g CO_2-eq / kWh is thus far wider than the difference between the two systems examined here, and a substantial part of it is an artefact of how the lifetime electricity output was estimated rather than a property of the installations.

No published assessment was found that relates substructure emissions to a structural quantity such as load-bearing capacity. The indicator introduced in Section 2.3 therefore cannot be benchmarked against the literature at present. Its value lies in enabling such comparisons in future work, and the three data points reported here provide a first reference range.

4.3 Limitations

Maintenance was not included (Section 2.2). Cleaning, component replacement and inspection trips would add to all three systems, with no reason to expect the omission to favour one concept.

The degradation rates were derived from the manufacturers' linear performance warranties. Warranted values are lower bounds on the remaining power and therefore upper bounds on the degradation rate, so the specific emissions reported here are conservative (Jordan and Kurtz, 2013). The same derivation was applied to all three systems, which keeps the comparison consistent.

The flat system loss of 10% is an assumption rather than a measured quantity. It was set below the simulation default because the default already contains an allowance for module degradation, which is applied explicitly here.

The load-bearing capacity was derived assuming complete submersion of the buoyancy bodies and therefore describes a theoretical maximum. Real installations operate with a substantial reserve. Since the same convention is applied to all three systems, the comparison is unaffected, but the absolute values should not be read as operating limits. The payload ratio reported in Tab. 2 is more sensitive to these conventions than the emission indicator, because the dead weight enters it directly rather than as a correction to a much larger displaced mass.

The two commercial systems were built in different years and carry different module generations. As set out in Section 2.3, this is precisely why the substructure indicator was introduced, and it remains a limitation of the system-level results reported in Section 3.1.

The prototype is documented less completely than the two commercial systems. The transport of the pre-assembled unit to the site is not included in its inventory, and its system-level results are therefore not reported. Its substructure data are nevertheless comparable, because the indicator does not depend on transport or operation.

The prototype lies 15.4% below FPV1, a clearer margin than the buoyancy calculation alone would support, since that calculation still rests on full submersion and on treating the corrugated pipes as smooth cylinders. The robust finding of this study remains the distance between FPV2 and the two other systems.

Finally, three installations in one region cannot support general conclusions about floating photovoltaic construction. They do, however, span three distinct structural concepts and load-bearing capacities differing by a factor of 46, which is sufficient to demonstrate that the indicator discriminates between designs.

5. Conclusion

Two commercial floating photovoltaic systems in North Rhine-Westphalia were assessed by life cycle assessment, complemented by a small-scale prototype. Over a 20-year service life the systems cause 120.2 and 87.7 g CO_2-eq / kWh. PV modules dominate both footprints, and the floating substructure and the modules contribute in roughly equal parts to the difference between the systems.

Because the module contribution is governed by the supply chain and by the module generation installed rather than by the structural concept, an additional indicator was introduced that relates the emissions of the floating substructure to its load-bearing capacity. On this basis the steel design requires 862.1 g CO_2-eq / kg, the steel–HDPE design 398.6 g CO_2-eq / kg and the prototype 729.1 g CO_2-eq / kg. The indicator is independent of site and of an assumption regarding energy yield.

The three systems distribute the structural work in fundamentally different ways. In FPV1 the steel bodies provide buoyancy and carry the loads at the same time, whereas FPV2 and the prototype assign these tasks to separate components. The prototype shows that separation alone is not sufficient. Its supporting structure is separated but built from aluminium, and it therefore stays closer to the steel design than its concept would suggest. The indicator makes the consequences of these concepts measurable on a common basis, which system-level results do not.

Future work should extend the indicator to further installations, so that the reference range reported here can be broadened, and should combine it with the durability of the materials involved. A substructure that provides carrying capacity at low emissions but requires earlier replacement would not be preferable, and the service life of floating structures under real conditions is still poorly documented.

References

Bucher, C., Wandel, J., Joss, D., 2022. Life expectancy of PV inverters and optimizers in residential PV systems, in: 8th World Conference on Photovoltaic Energy Conversion (WCPEC-8), Milan, Italy. p. 3DV.1.46. doi:10.24451/arbor.18138.

Cagle, A.E., Armstrong, A., Exley, G., Grodsky, S.M., Macknick, J., Sherwin, J., Hernandez, R.R., 2020. The land sparing, water surface use efficiency, and water surface transformation of floating photovoltaic solar energy installations. Sustainability 12, 8154. doi:10.3390/su12198154.

Cazzaniga, R., Cicu, M., Rosa-Clot, M., Rosa-Clot, P., Tina, G.M., Ventura, C., 2018. Floating photovoltaic plants: Performance analysis and design solutions. Renewable and Sustainable Energy Reviews 81, 1730–1741. doi:10.1016/j.rser.2017.05.269.

Cromratie Clemons, S.K., Salloum, C.R., Herdegen, K.G., Kamens, R.M., Gheewala, S.H., 2021. Life cycle assessment of a floating photovoltaic system and feasibility for application in Thailand. Renewable Energy 168, 448–462. doi:10.1016/j.renene.2020.12.082.

Ecoinvent Association, 2025. ecoinvent database, version 3.12. https://ecoinvent.org. Accessed 10 March 2026.

European Commission, 2022. Environmental footprint method, version 3.1. https://eplca.jrc.ec.europa.eu/EnvironmentalFootprint.html. Accessed 10 March 2026.

European Commission, 2025. PVGIS – photovoltaic geographical information system. https://re.jrc.ec.europa.eu/pvg_tools/en/. Accessed 10 March 2026.

Federal Republic of Germany, 2023. Wasserhaushaltsgesetz (WHG), section 36: Installations in, on, over and under surface waters. Federal Water Act, as amended with effect from 1 January 2023.

Fraunhofer Institute for Solar Energy Systems ISE, 2026. Photovoltaics Report. Technical Report. Fraunhofer ISE. Freiburg. Updated 14 July 2026, accessed 17 August 2026.

Frehner, A., Stucki, M., Itten, R., 2024. Are alpine floatovoltaics the way forward? life-cycle environmental impacts and energy payback time of the world's first high-altitude floating solar power plant. Sustainable Energy Technologies and Assessments 68, 103880. doi:10.1016/j.seta.2024.103880.

Gandhi, O., Rodríguez-Gallegos, C.D., Ting, S.A., Rahman, T., Vinayagam, L., Sun, H., Ali, J.M.Y., Yagli, G.M., Alvarez-Alvarado, M.S., Pillai, D.S., Lin, F., Reindl, T., 2026. Design and implementation of floating photovoltaics. Nature Reviews Clean Technology 2, 414–432. doi:10.1038/s44359-026-00171-4.

International Organization for Standardization, 2006a. ISO 14040: Environmental management – life cycle assessment – principles and framework. ISO, Geneva.

International Organization for Standardization, 2006b. ISO 14044: Environmental management – life cycle assessment – requirements and guidelines. ISO, Geneva.

Jordan, D.C., Kurtz, S.R., 2013. Photovoltaic degradation rates – an analytical review. Progress in Photovoltaics: Research and Applications 21, 12–29. doi:10.1002/pip.1182.

Kester, J., Liu, J., Binani, A., 2024. Carbon footprint analysis of floating PV systems. Technical Report IEA-PVPS T12-29:2024. IEA Photovoltaic Power Systems Programme, Task 12.